Effect of wire length on quantum coherence in InGaAs wires

Yuantao Xie

SZU-NUS Collaborative Innovation Center for Optoelectronic Science and Technology,
International Collaborative Laboratory of 2D Materials for Optoelectronics Science and Technology of Ministry of Education,
College of Optoelectronic Engineering, Shenzhen University, Shenzhen 518060, China

J. J. Heremans[*]
Department of Physics, Virginia Tech, Blacksburg, Virginia 24060, USA

Quantum phase coherence lengths were experimentally measured in nanolithographic wires to investigate the effects of wire length on quantum decoherence, which can be limited by mechanisms such as coupling to an external classical environment. The work demonstrates that device geometry and coupling to the environment have to be taken into account in quantum coherence, of relevance in quantum technologies using electronic nanostructures. The low-temperature measurements of the quantum phase coherence lengths use quantum transport, specifically antilocalization, on wires fabricated from an InGaAs/InAlAs heterostructure. It is observed that longer wire lengths result in longer quantum phase coherence lengths, tending to an asymptotic value in long wires. The results are understood from the observation that longer wires average out the quantum decoherence introduced at the end sections by coupling to the external environment. The experimental results are quantitatively compatible with a model expressing reduced backscattered amplitude due to quantum interference at the wire ends.

I. INTRODUCTION

The study of quantum coherence of charge carriers in the solid state has attracted increasing attention for the insights it provides into the fundamental properties of quantum systems and into quantum measurement theory, and for the importance it carries for the field of quantum information processing. Solid-state systems that are larger than the atomic scale but still of a length scale preserving quantum phenomena, constitute a ready platform to study mechanisms limiting quantum coherence of electrons. Such solid-state quantum systems find distinctive use as nanoelectronic devices, and hence quantum electronic transport approaches, as used in this work, are in this application intrinsically suited to study quantum coherence. In particular, the spatial extent along which quantum coherence is maintained in mesoscopic conducting wire geometries is of relevance today due to the interest in hybrid semiconductor-superconductor nanowires for the study of solid-state Majorana quasiparticles, where the Majorana states are localized at the ends of a wire, along the length of which quantum coherence of the Majorana states must be preserved [1,2]. The carrier quantum phase coherence length L_ϕ is defined as an average length scale over which quantum coherence is maintained and thus beyond which the relative quantum phases of the carrier states are randomized. In mesoscopic electronic systems several decoherence mechanisms limit L_ϕ. Among these are inelastic or quasielastic scattering mechanisms such as electron-phonon and electron-electron scattering [3–5]. Decoherence can also result from energy level broadening beyond the Thouless energy, thermally or due to excitation voltages or currents, causing averaging over independent and incoherent channels [6]. At low temperature T, many decoherence mechanisms dependent on energy exchange are suppressed [5,7], and L_ϕ reaches values sufficiently long to study electronic transport phenomena relying on quantum interference in nanoscale and mesoscopic devices [6,8]. Yet geometrical effects also play a role [9], e.g., via environmental coupling decoherence [4,7,10–13] originating from the fact that measurement of a quantum system necessitates coupling to the external environment, taken as a classical system [7,10,14,15]. Environmental coupling decoherence can be regarded as the effect of dynamical degrees of freedom disregarded in the definition of the original Hamiltonian describing the quantum state and added in retrospect to more completely define the state. The present work demonstrates the general importance of device geometry—particularly wire length—and of environmental coupling decoherence in studying and using quantum-coherence phenomena, among others in the characterization of new quantum states of matter realized in nanoscale systems. Previous studies relating to the dependence of quantum decoherence on device geometry and size have been performed in quantum wires [16–24], quantum rings [25–27], quantum ring arrays or cylinders [3,28–30], and quantum dots [9,12,31–33].

In this work parallel arrays of wires of various lengths were fabricated on an InGaAs/InAlAs heterostructure. The heterostructure is essentially free of any magnetic impurities and is thus a good host for studying intrinsic decoherence mechanisms [12,33]. Each wire array consists of 20 parallel quasi-one-dimensional (Q1D) wires of given wire length L. Q1D denotes that the conducting wire width W is shorter than
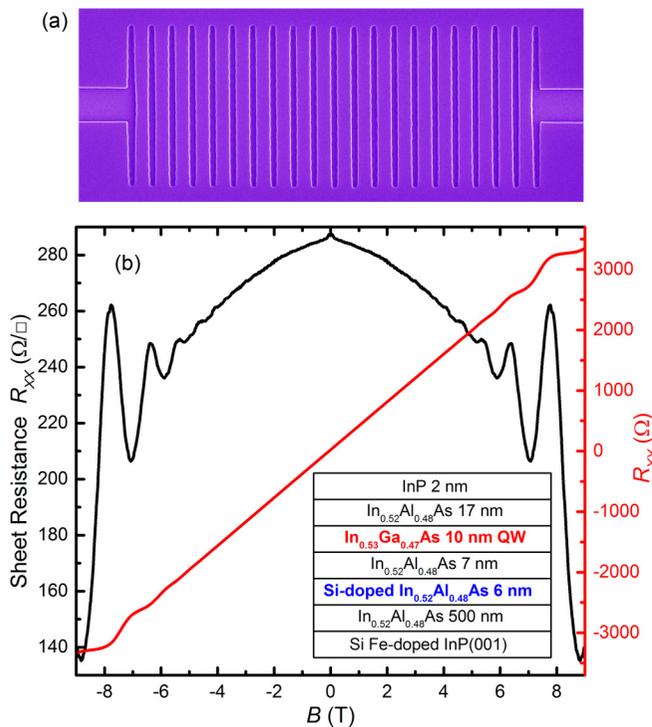
*heremans@vt.edu

FIG. 1. (a) Scanning electron micrograph of a typical array of parallel wires, here with $L = 11.0$ μm. Etched trenches (darker regions) form insulating barriers for the 2DES, thus delineating the conducting wires. The lithographic wire width is 0.70 μm for all wires. (b) R_{XX} (black) and R_{XY} (red) at 0.38 K on a Hall bar fabricated on the InGaAs/InAlAs heterostructure, with the heterostructure layer sequence depicted in the inset.

the mobility mean-free-path and than L_ϕ, but substantially larger than the Fermi wavelength λ_F such that lateral quantization and subband transport physics can be neglected. L_ϕ as a measure of quantum coherence is in this work extracted as a function of L and T by the quantum interference effect of weak antilocalization (WAL) [19,21,34–37]. As a quantum interference effect, WAL is a sensitive probe of quantum coherence and originates in quantum coherence corrections to the conductance, caused by interference between backscattered time-reversed electron trajectories. The interference leads to a conductance with a characteristic dependence on the magnetic field B applied normally to the surface, as modified (in the case of WAL) by strong spin-orbit interaction (SOI) [38]. Due to the existence of SOI in the InGaAs/InAlAs heterostructure, analysis of the characteristic magnetoresistance due to WAL affords a path to extract values for L_ϕ. The WAL correction depends on the random quantum phase accumulated over the time-reversed trajectories, leading to a sensitivity of the magnetoresistance to

L_ϕ. In mesoscopic geometries communicating with the wider environment, the WAL correction also depends on the return probability of those time-reversed pairs that originate in the geometry and partially sample the environment [18,39,40]. Given the relatively higher importance of such trajectories in shorter wires, the smaller average return probability at the end of shorter wires tends to reduce L_ϕ in shorter wires when compared to longer wires. The lower return probability equates to decoherence due to coupling to the environment. Coupling to the environment can equivalently be expressed in terms of a dwell time τ_d in the mesoscopic structure, with shorter τ_d equivalent to stronger coupling and associated with shorter quantum phase coherence time τ_ϕ. Previous work [12,33] has noted that a larger lateral quantum dot size leads to a longer τ_ϕ, explained by invoking τ_d proportional to system size, limiting τ_ϕ at low T. A longer $L_\phi = \sqrt{D\tau_\phi}$ (where D denotes the carrier diffusion coefficient) is then expected in systems of larger size such as in longer Q1D wires. In the present experiments, L_ϕ indeed has a positive correlation with L over a range of T, consistent with environmental coupling decoherence quantifiable using WAL. The dependence of L_ϕ on T in the present experiments is consistent with Nyquist scattering due to quasielastic electron-electron interactions [5,28,29,41], a main decoherence source at low T. In Nyquist scattering a random phase is accumulated by the fluctuations of the electromagnetic field generated by the other electrons.

II. MATERIAL AND SAMPLE PROPERTIES

Hall bar mesas were defined on the InGaAs/InAlAs heterostructure by photolithography and wet etching, and subsequently arrays of 20 parallel Q1D wires were defined on the mesas by electron-beam lithography and wet etching [Fig. 1(a)]. Wire lengths were $L = 4.0$ μm, 6.0 μm, and 11.0 μm, with lithographic width $W_{\text{lith}} = 0.70$ μm (Table I). As quantified below from the measured wire resistance, the effective conducting width W is narrower than W_{lith} due to side etching and existence of a depletion layer. A typical set of Q1D wires is depicted in the micrograph of Fig. 1(a). Measuring a large number of wires in parallel (here $N = 20$) suppresses universal conductance fluctuations, the amplitude of which scales as $1/\sqrt{NLW}$ [42]. The suppression is beneficial, since strong universal conductance fluctuations can impede the WAL analysis. The longitudinal magnetotransport coefficient R_{XX} and the Hall coefficient R_{XY} as measured on a macroscopic Hall bar at $T = 0.38$ K are depicted vs B in Fig. 1(b), showing Shubnikov-de Haas oscillations and an incipient integer quantum Hall effect at higher B. The inset of Fig. 1(b) contains the heterostructure layer sequence, which was grown by molecular-beam epitaxy on semi-insulating InP (001) substrate. From bottom to top the lattice-matched

TABLE I. Lengths and lithographic widths of the wires, quantum phase coherence lengths at $T = 0.38$ K, and exponent p of the T dependence of the quantum decoherence rate for T varying from 1.0 K to 10.0 K.

Wires	$L = 11.0$ μm $W_{\text{lith}} = 0.70$ μm	$L = 6.0$ μm $W_{\text{lith}} = 0.70$ μm	$L = 4.0$ μm $W_{\text{lith}} = 0.70$ μm
L_ϕ (μm)	1.42	1.27	1.04
$\tau_\phi^{-1} \sim T^p$	$p = 0.690 \pm 0.030$	$p = 0.679 \pm 0.056$	$p = 0.716 \pm 0.052$

layer sequence consists of a 500 nm $In_{0.52}Al_{0.48}As$ buffer, a 6 nm Si-doped $In_{0.52}Al_{0.48}As$ layer, a 7 nm $In_{0.52}Al_{0.48}As$ spacer, the 10 nm wide $In_{0.53}Ga_{0.47}As$ electron quantum well (QW), a 17 nm $In_{0.52}Al_{0.48}As$ spacer, and a 2 nm undoped InP cap layer. Electrons are provided to the QW by 6 nm Si-doped $In_{0.52}Al_{0.48}As$, and the two-dimensional electron system (2DES) is hosted in QW with areal carrier density $N_s = 1.58 \times 10^{16}$ m^{-2} as determined on the Hall bar at $T = 0.38$ K from both R_{XY} and Shubnikov-de Haas oscillations [Fig. 1(b)]. The unpatterned 2DES' sheet resistance is obtained as $R_{\square 2D} = \frac{1}{N_s e \mu_{2D}} = 287$ $\Omega/\square$, with mobility $\mu_{2D} = 1.38$ m^2/(Vs). In the range 0.38 K $\leqslant T \leqslant 10.0$ K of the measurements both μ_{2D} and N_s do not vary significantly. Other parameters depending on μ_{2D} and N_s are evaluated accounting for nonparabolicity in the InGaAs conduction band [43,44], with a ratio of Γ-point effective mass m^* to free-electron mass of 0.0353 and a low T band gap of $E_g = 813$ meV. In the unpatterned 2DES we have the elastic scattering time $\tau_{e2D} = 0.81$ ps, the mean-free-path $\ell_{e2D} = 0.59$ μm, the Fermi energy $E_F = 80.4$ meV, $\lambda_F = 19.9$ nm ($\ll W$), and the diffusion constant $D_{2D} = 0.11$ m^2/s. D_{2D} is calculated using the 2D degenerate expression $D = \frac{1}{2} v_F \ell_{e2D}$, where v_F is the Fermi velocity derived from N_s. Situating the $In_{0.52}Al_{0.48}As$ doping layer below the $In_{0.53}Ga_{0.47}As$ QW results in asymmetry in the QW confinement potential for the 2DES and in a substantial SOI, yet also depresses μ_{2D} compared with other $In_{0.53}Ga_{0.47}As/In_{0.52}Al_{0.48}As$ heterostructures [45,46]. Measurements occurred in a ^{3}He cryostat using four-contact low-frequency lock-in techniques under constant current $I = 20$ nA, sufficiently low to avoid heating the 2DES. For each array of parallel wires, the measured magnetoresistance $R_m(B)$ includes a magnetoresistance $R(B)$ of each of the 20 identical wires in the array and a series magnetoresistance of the unpatterned 2DES regions. Hence $R_m(B) = \frac{R(B)}{20} + \frac{L_{2D}}{W_{2D}} R_{\square 2D}(B)$, where L_{2D} and W_{2D} are the dimensions of the unpatterned regions known from pattern design, and the unpatterned sheet magnetoresistance $R_{\square 2D}(B)$ is measured on the Hall bar. $R(B)$ is then obtained as $R(B) = 20(R_m(B) - \frac{L_{2D}}{W_{2D}} R_{\square 2D}(B))$, and $R(B)$ yields the wire magnetoconductance $G(B) = 1/R(B)$ required for WAL analysis. As an example, Fig. 2 shows $\Delta G(B) = G(B) - G(B=0)$ for the 6.0 μm wires at T from 0.38 K to 10.0 K. The sharp negative magnetoconductance for $B \lesssim 12$ mT followed by a positive magnetoconductance is characteristic of WAL.

The following discussion introduces the WAL analysis appropriate for Q1D wires. The quantum correction to the 2D conductivity $\sigma_{2D} = (L/W)G$ is proportional to the length over which a wave packet retains coherence. In the absence of SOI for a system of width W at $B = 0$ the quantum correction per spin channel $\delta\sigma_{2D}$ is expressed as [42,47]:

$$\delta\sigma_{2D} = -\frac{1}{2} \frac{e^2}{\pi \hbar} \frac{L_\phi}{W}. \quad (1)$$

Under applied B, the Aharonov-Bohm phases for time-reversed paths differ in sign, and hence time-reversal symmetry breaking due to the accumulation of Aharonov-Bohm phases will reduce the effective coherence length. An effective time-reversal symmetry breaking length known as the magnetic length L_B is introduced, which forms a limit for the effective
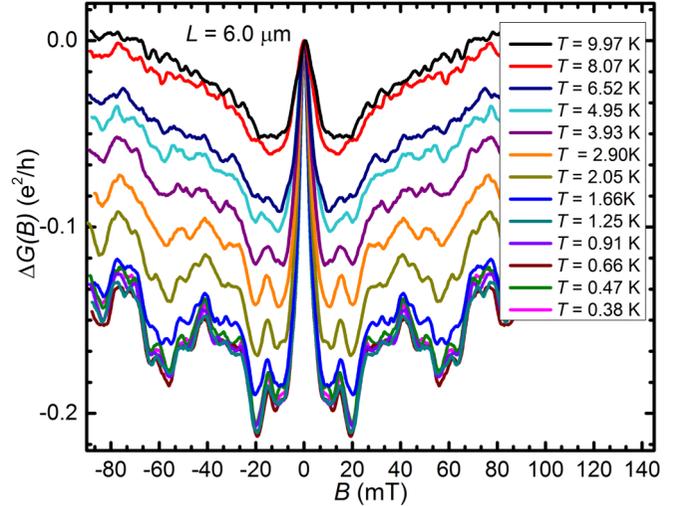

FIG. 2. Magnetoconductance $\Delta G(B)$ vs B for the wires with $L = 6.0$ μm parametrized in T.

coherence length $1/\sqrt{L_\phi^{-2} + L_B^{-2}}$. The effect of L_B is to delay accumulation of a magnetic flux and its associated Aharonov-Bohm phase to higher B in a narrow wire, and hence to spread out the magnetoresistance features over higher B. The Aharonov-Bohm phase weakens the constructive interference of time-reversed paths and leads to the negative magnetoresistance characteristic of weak localization. Under SOI however, the effective vector potential due to SOI also introduces spin-dependent Aharonov-Casher phase shifts, leading to spin decoherence (properly dephasing) with a characteristic length scale L_{so} [48]. The pairing of time-reversed trajectories (Cooperons) then leads to singlet and triplet contributions to the quantum correction $\delta\sigma_{2D}$. Under SOI L_ϕ is thus replaced by a combination of length scales categorized as singlet and triplet lengths [19,21,47–52]. The singlet length scale $L_{0,0}$ is expressed as:

$$L_{0,0} = \left(L_\phi^{-2} + L_B^{-2}\right)^{-\frac{1}{2}}. \quad (2)$$

The singlet $L_{0,0}$ does not contain L_{so} and is not sensitive to spin decoherence under SOI since the corresponding total spin adds to zero [19,21,48,52]. Only L_ϕ and L_B limit $L_{0,0}$. The triplet length scales $L_{1,m}$ ($m = \pm 1, 0$) are expressed as:

$$L_{1,\pm 1} = \left(L_\phi^{-2} + L_{so}^{-2} + L_B^{-2}\right)^{-\frac{1}{2}}$$
$$L_{1,0} = \left(L_\phi^{-2} + 2L_{so}^{-2} + L_B^{-2}\right)^{-\frac{1}{2}}. \quad (3)$$

The difference between $L_{1,\pm 1}$ and $L_{1,0}$ lies in anisotropic spin decoherence in 2D systems [34] and does not exist in 3D systems [47,51]. The triplet contributions to $\delta\sigma_{2D}$ will be negative (leading to positive magnetoconductance) while the singlet contribution will be positive and will reverse weak localization to WAL (negative magnetoconductance at low B). In wide, laterally unconstrained 2D systems, $L_B = l_m \equiv \sqrt{\hbar/eB}$. When the 2DES is narrowed to a Q1D wire with $W \lesssim l_m$ the accumulation of Aharonov-Bohm phases is impeded (equivalently, the wave function boundary conditions are modified). If also the mean-free-path $\gtrsim 0.6 W$, ballistic magnetic flux cancellation has to be considered due to self-crossing of
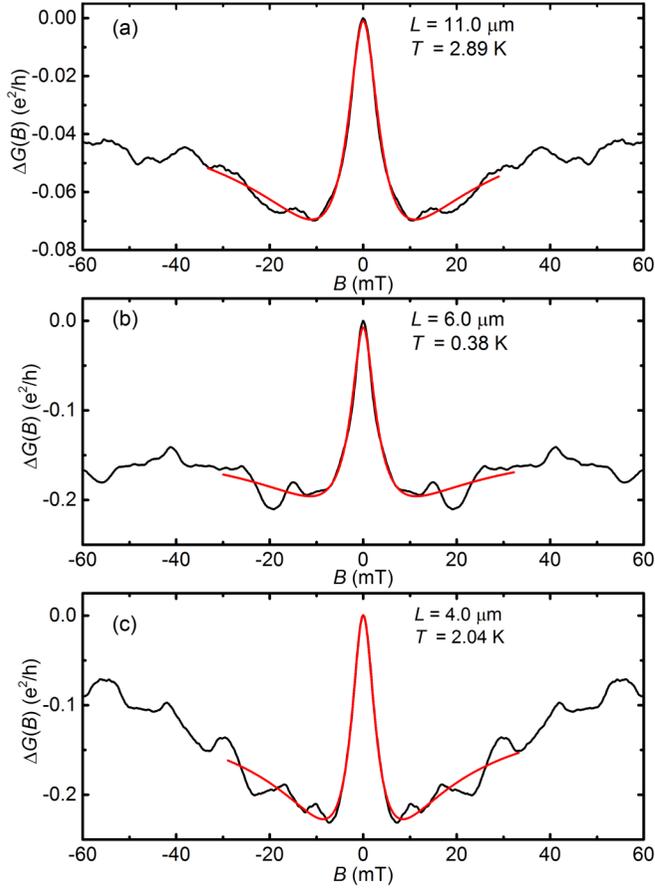
FIG. 3. (a) Magnetoconductance $\Delta G(B)$ vs B for wire with $L = 11.0$ μm at $T = 2.89$ K [data in black, fitting of Eq. (6) in red]. (b) Magnetoconductance $\Delta G(B)$ vs B for wire with $L = 6.0$ μm at $T = 0.38$ K [data in black, fitting of Eq. (6) in red]. (c) Magnetoconductance $\Delta G(B)$ vs B for wire with $L = 4.0$ μm at $T = 2.04$ K [data in black, fitting of Eq. (6) in red].

time-reversed trajectories in narrow wires. Considered together, for low B, L_B is then modified to [19,21,29,48,53]:

$$L_B = l_m \sqrt{\frac{C_1 l_m^2 \ell_{e1D}}{W^3}}. \qquad (4)$$

Here $C_1 = 4.75$ for specular boundary scattering and $C_1 = 2\pi$ for diffusive boundary scattering [19,21,53], while ℓ_{e1D} is the mean-free-path in the Q1D wire. From Eq. (1), the quantum correction $\delta\sigma_{2D}$ is finally expressed as:

$$\delta\sigma_{2D} = -\frac{1}{2}\frac{e^2}{\pi\hbar}\frac{1}{W}\left(\sum_{m=0,\pm 1} L_{1,m} - L_{0,0}\right). \qquad (5)$$

The measured conductance correction $\delta G(B) = G(B) - G_0$, is related to $\delta\sigma_{2D}$ by $\delta G(B) = (W/L)\delta\sigma_{2D}$, with G_0 the classical conductance of the wire ($G_0 \neq G(0)$ due to the effects of L_ϕ and L_{so}). The dependence of $\delta G(B)$ on B thus reduces to a combination of length ratios [19,21,47,48,51]:

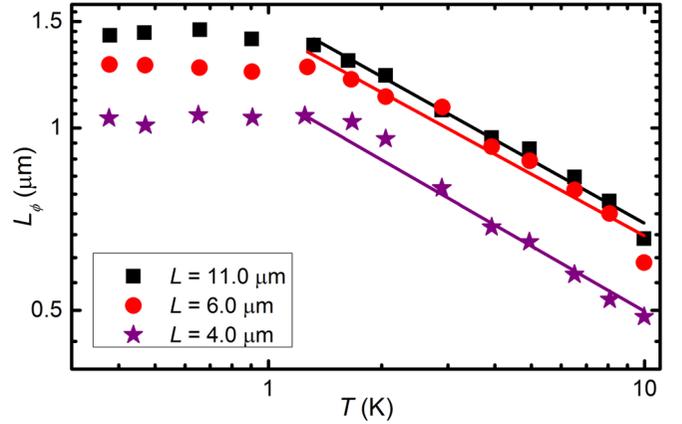$$\delta G(B) = -\frac{1}{2}\frac{e^2}{\pi\hbar}\frac{1}{L}(L_{1,+1} + L_{1,-1} + L_{1,0} - L_{0,0}). \qquad (6)$$

FIG. 4. Phase coherence lengths, L_ϕ vs T extracted from $\Delta G(B)$ using 1D WAL analysis for the Q1D wire sets with $L = 4.0$ μm, 6.0 μm, and 11.0 μm. Solid lines for $T > 1$ K represent fits to $L_\phi \sim T^{-p/2}$ with values for p as listed in Table I.

The experimental data can be directly compared to fits to Eq. (6) since $\Delta G(B) = G(B) - G(0) = \delta G(B) - \delta G(0)$. With the presence of an electronic depletion layer in InGaAs structures, a smooth potential is formed at the wire edges, and we expect boundary scattering to be specular. Hence $C_1 = 4.75$ is used [21,53,54]. Values for L_ϕ, L_{so}, and ℓ_{e1D} [entering in Eq. (4)] are used as fitting parameters to fit the experimental data for $\Delta G(B)$ to Eq. (6). It is to be noted that similarly to previous work [21], we expect $\ell_{e1D} < \ell_{e2D}$, a drop in electron mean-free-path in the wire compared to the unpatterned 2DES (in Ref. [21] equivalently expressed via a drop in D). The WAL analysis depends on ℓ_{e1D} and on W, neither of which are known a priori. While ℓ_{e1D} is obtained as a fitting parameter, W can be calculated as follows. A first estimate W_0 is obtained by assuming the sheet resistance in the wires $R_{\square 1D}$ equals $R_{\square 2D}$, and using $R_{B=0} = \frac{L}{W_0}R_{\square 2D}$ at $T = 0.38$ K. By a least squares fitting over L, we obtain $W_0 = 0.34$ μm. By using the known wire resistance $R = \frac{\hbar}{e^2}\sqrt{\frac{2\pi}{N_s}}\frac{L}{W\ell_{e1D}}$ and assuming constant N_s, we obtain $W \rightarrow \frac{\ell_{e2D}}{\ell_{e1D}}W_0$. By consistent fitting over the three wire sets, we arrive at $\ell_{e1D} = 0.50$ μm and $W = 0.41$ μm, common to the three wire sets.

III. DATA ANALYSIS AND RESULTS

Figure 3 depicts examples of fits of Eq. (6) to $\Delta G(B)$ for the Q1D wires with $L = 11.0$ μm, 6.0 μm, and 4.0 μm. It is apparent that the model captures the experiments well. The fluctuations in magnetoconductance are due to universal conductance fluctuations surviving the averaging process, aggravated by the subtraction of the series resistance of unpatterned areas and the calculation of the magnetoconductance correction $\Delta G(B)$. Since the characteristic magnetoresistance due to WAL occurs predominantly at lower B, the fitting is not affected by the fluctuations.

In Fig. 4 the extracted L_ϕ is plotted vs T, parametrized in L. Prior to discussing the dependence of L_ϕ on L and T, we briefly discuss Fig. 5 where extracted fitting values of L_{so} are plotted vs T, parametrized in L. Values for L_{so} vary from ~ 0.4 μm to 0.2 μm over the ranges of L and T,
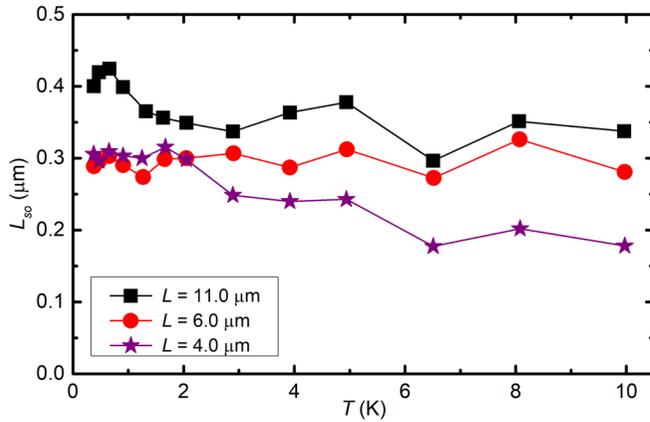
FIG. 5. Spin coherence lengths due to spin-orbit interaction, L_{so} vs T extracted from $\Delta G(B)$ using 1D WAL analysis for the Q1D wire sets with $L = 4.0\,\mu m$, $6.0\,\mu m$, and $11.0\,\mu m$. Lines are guides to the eye.
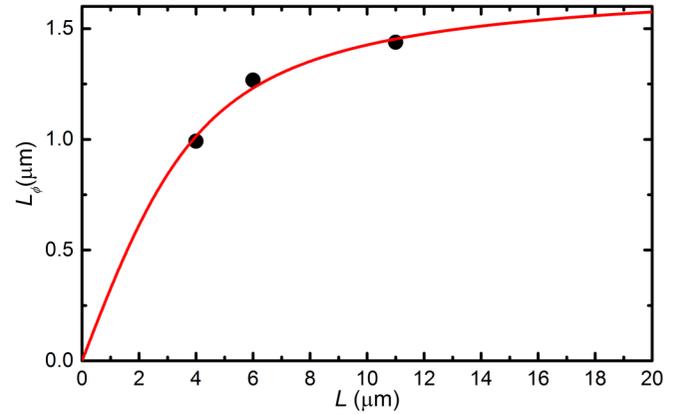

FIG. 6. Phase coherence lengths L_ϕ vs L at $T = 0.38$ K. Black dots are data, the red line represents the fit to Eq. (7) with $L_{\phi\infty} = 1.73\,\mu m$.

short lengths compatible with expectations for a 2DES with substantial SOI. A systematic dependence of L_{so} on L cannot readily be concluded, although it is tentatively observed that L_{so} increases with increasing L. A weak decrease of L_{so} with increasing T is noted for $L = 4.0\,\mu m$ and $L = 11.0\,\mu m$. The weak decrease with increasing T was previously observed [16,20,21] and hitherto not fully explained.

Figure 4 shows that L_ϕ decreases with increasing T, in agreement with other work, both theoretical and experimental [4,5,19,20,55,56]. At lower $T < 1$ K a saturation of L_ϕ appears, also previously observed and discussed [5,19,20,57–61]. While the origin of the saturation is under debate, several causes can be ruled out in our experiments. Magnetic impurities possibly present in metal samples are typically absent in semiconductor heterostructures grown by molecular-beam epitaxy [12,33]. To rule out thermal causes due to sample current, we measured the wire magnetoresistance at $T = 0.38$ K with $10\,$nA $\leqslant I \leqslant 100\,$nA. The magnetoresistance remained identical for $10\,$nA $\leqslant I \leqslant 50\,$nA, and at $100\,$nA showed a smaller WAL amplitude, implying that for $I \leqslant 50\,$nA electron heating can be neglected. Present results were all measured at $I = 20\,$nA. Further, T in the measurement system is calibrated using a Dingle analysis of Shubnikov-de Haas oscillations in a high-mobility 2DES in GaAs/AlGaAs. The analysis of Shubnikov-de Haas oscillations can also largely rule out nonequilibrium electrical noise [62] (e.g., injected into the sample via the wiring and the measurement system) as a dominant source of decoherence in the range of T of the experiments. Indeed what is measured via Shubnikov-de Haas oscillations [63,64] is the broadening of quantum levels, specifically Landau levels, due to either thermal effects or electrical noise by an amount $\sim \hbar/\tau_\phi$. Electrical noise would likely limit the visibility of Shubnikov-de Haas oscillations as well as the visibility of WAL, because in both cases quantum levels would be broadened by the electrical noise by $\sim \hbar/\tau_\phi$. Since the value of the effective T indicated by Shubnikov-de Haas analysis is a measure of the level broadening, Shubnikov-de Haas analysis would register a lowering of τ_ϕ due to electrical noise as a discrepancy between the measured T and the effective T experienced by the 2DES in a sample. The

saturation of L_ϕ is not the focus of the present work and won't be discussed hereunder. A drop in L_ϕ with increasing T for all samples is present in Fig. 4 for $T > 1$ K. Analysis shows that for $T > 1$ K, the results fit $L_\phi \sim T^{-p/2}$ with $p/2 \approx 0.34 \pm 0.02$, leading to a decoherence rate $\tau_\phi^{-1} \sim T^p$ with $p \approx 0.69 \pm 0.03$. Values for p are listed in Table I. The dependence on T of τ_ϕ^{-1} can have several causes. Electron-phonon scattering leads to a decoherence rate $\tau_{ep}^{-1} \sim T^q$ with q experimentally determined as $2 \ldots 4$ [5,20]. Electron-electron scattering [4,5,20,31] with large energy transfer leads to a decoherence rate $\tau_{ee}^{-1} \sim T^2$ in 1D and 2D, while quasielastic Nyquist scattering leads to a decoherence rate $\tau_N^{-1} \sim T^{2/3}$ in 1D [20,61] and $\tau_N^{-1} \sim T$ in 2D [4,31,42,65]. Averaging of transport phenomena over incoherent channels, expressed as broadening of energy levels beyond the Thouless energy, leads to a decoherence rate $\tau_T^{-1} \sim T^{1/2}$, and can result from thermal effects or excitation by applied voltages or currents [6]. For the Q1D wires by fitting $L_\phi \sim T^{-p/2}$, we obtain $p = 0.69, 0.68$, and 0.72, respectively (Table I), consistent with Nyquist scattering in 1D with $\tau_N^{-1} \sim T^{2/3}$. An analysis of L_ϕ on the unpatterned 2DES in the Hall bar (not shown) shows $L_\phi \sim T^{-p/2}$ with $p \approx 1.04$, consistent with a 2D Nyquist decoherence rate $\tau_N^{-1} \sim T$. According to discussion above and results in Fig. 4, we can conclude that quasielastic Nyquist scattering plays a role in limiting L_ϕ in our samples.

Figure 4 shows that L_ϕ maintains a positive correlation with L, whereby as L increases, L_ϕ also increases. The saturated values of L_ϕ for $T < 1$ K obey the same dependence on L as observed over 0.38 K $< T < 10.0$ K. For $T < 1$ K, L_ϕ of the wire with $L = 11.0\,\mu m$, reaches $1.42\,\mu m$, substantially longer than $L_\phi = 1.04\,\mu m$ for the wire with $L = 4.0\,\mu m$. Figure 6 shows the L_ϕ measured at $T = 0.38$ K (saturated value) plotted vs L. The positive correlation of L_ϕ with L finds an explanation in the interaction of the quantum states in the wires with the classical environment [18,39]. With the wires connected to the environment, taken as a macroscopic classical system, environmental coupling decoherence is introduced at the endpoints of the wires, while the decoherence is weaker into the wires away from the endpoints. Averaging over L then shows that shorter wires are more sensitive to environmental coupling decoherence and will exhibit shorter L_ϕ.

The dependence of L_ϕ on both L and on T in Fig. 4 point to the importance of geometrical effects, expressed in environmental coupling decoherence. In general, the observations illustrate the sensitivity of quantum coherence in nanoscale structures to interactions with wide neighboring regions. Environmental coupling decoherence can be quantified using a dwell time τ_d, via a total decoherence rate given by $\tau_\phi^{-1} = \tau_{\phi 0}^{-1} + \tau_d^{-1}$. The term $1/\tau_d$ quantifies an escape rate out of the quantum system, associated with environmental coupling, and hence denotes the environmental decoherence rate. The term $1/\tau_{\phi 0}$ equals the decoherence rate for an isolated system where $\tau_d \to \infty$. The dwell time has been invoked for decoherence in lateral quantum dots [12,33], while experiments show that the wider the aperture connecting the quantum dots to the environment, the shorter is τ_ϕ due to shorter τ_d [7,13]. In the present wires it is possible that the limit imposed on τ_ϕ by τ_d is responsible for the saturation of L_ϕ at low T, where other decoherence mechanisms play a lesser role.

The effect of environmental decoherence (and equivalently of τ_d) on the effectively measured L_ϕ in a wire of length L can be quantified using expressions derived for the backscattered amplitude of a diffusing electron due to quantum interference [18,39,40]. This approach bears a close similarity to the concept of escape rate, in that an electron diffusing from the wire into the wide 2D connecting regions at the endpoints of the wire, thereby escaping the quantum system, has a reduced probability of returning to its starting point and contributing to the quantum interference correction to conductance. Assuming perfect contacts between the wire and the wide 2D connecting regions at the endpoint, such that the backscattering amplitude for an electron diffusing into the environment is zero, one obtains [19,39]:

$$L_\phi = L_{\phi\infty}\left(\coth\left(\frac{L}{L_{\phi\infty}}\right) - \frac{L_{\phi\infty}}{L}\right). \qquad (7)$$

Here L_ϕ denotes the effectively measured coherence length in a wire of length L, and $L_{\phi\infty}$ denotes the coherence length in a wire with $L \to \infty$ for which interaction with the environment can be neglected. As depicted in Fig. 6, Eq. (7) can remarkably well reproduce the dependence of L_ϕ on L for the values of L in this work. The fit to the data yields $L_{\phi\infty} = 1.73\ \mu$m ($T = 0.38$ K). Since Nyquist scattering due to quasielastic electron-electron interactions dominates decoherence for $T \gtrsim 1.5$ K, it is expected that a value close to $L_{\phi\infty} = 1.73\ \mu$m will

result from the expression for Nyquist scattering evaluated for $T = 1.5$ K, at the onset of saturation of L_ϕ. For Q1D wires, L_ϕ limited by Nyquist scattering is theoretically described by [19,26,29]:

$$L_\phi = \sqrt{2}\left(\frac{\hbar^2 D_{1D}^2 g(E_F) W}{k_B T}\right)^{1/3} \qquad (8)$$

illustrating the characteristic dependence $L_\phi \sim T^{-1/3}$. Here $g(E_F)$ represents the 2D density of states at E_F, $D_{1D} \approx (\ell_{e1D}/\ell_{e2D})D_{2D}$ represents the diffusion constant in the wires, and k_B is Boltzmann's constant. A nonparabolic band approximation [43,44] predicts $g(E_F) = \frac{m^*}{\pi\hbar^2}(1 + \frac{2E_F}{E_g})$. Evaluation of Eq. (8) for $T = 1.5$ K then yields $L_\phi = 1.95\ \mu$m, indeed close to the value $L_{\phi\infty} = 1.73\ \mu$m derived from the measurements and Eq. (7). The consistency between the data in Fig. 4 and Fig. 6, with Eq. (7) and Eq. (8) strengthens the interpretation presented for the dependence of L_ϕ on L and T.

IV. CONCLUSIONS

In conclusion, quantum phase coherence lengths L_ϕ as a function of wire length L were obtained via a 1D WAL analysis, with ballistic transport corrections, for wires fabricated on a 2DES in a InGaAs/InAlAs heterostructure. It is observed that the measured L_ϕ increases with increasing L, effectively explained by the quantum decoherence effect introduced at the wire endpoints by environmental coupling. The decoherence effect of the coupling between the wire and the wide 2D connecting regions at the endpoints can be quantified by an expression for reduced coherent backscattering at the endpoints. The dependence of L_ϕ on T is consistent with the effects of quasielastic Nyquist scattering in the 1D regime. The work underlines the influence of sample geometry and interactions with external neighboring regions on quantum decoherence in nanostructures, with particular emphasis on decoherence in nanowires with relevance to the study of new quantum states of matter, and with relevance in quantum technologies.

[1] M. T. Deng, S. Vaitiekenas, E. B. Hansen, J. Danon, M. Leijnse, K. Flensberg, J. Nygard, P. Krogstrup, and C. M. Marcus, Science **354**, 1557 (2016).

[2] S. R. Elliott and M. Franz, Rev. Mod. Phys. **87**, 137 (2015).

[3] M. Ferrier, L. Angers, A. C. H. Rowe, S. Guéron, H. Bouchiat, C. Texier, G. Montambaux, and D. Mailly, Phys. Rev. Lett. **93**, 246804 (2004).

[4] B. Hackens, F. Delfosse, S. Faniel, C. Gustin, H. Boutry, X. Wallart, S. Bollaert, A. Cappy, and V. Bayot, Phys. Rev. B **66**, 241305(R) (2002).

[5] J. J. Lin and J. P. Bird, J. Phys.: Condens. Matter **14**, R501 (2002).

[6] S. L. Ren, J. J. Heremans, C. K. Gaspe, S. Vijeyaragunathan, T. D. Mishima, and M. B. Santos, J. Phys.: Condens. Matter **25**, 435301 (2013).

[7] J. P. Bird, A. P. Micolich, H. Linke, D. K. Ferry, R. Akis, Y. Ochiai, Y. Aoyagi, and T. Sugano, J. Phys.: Condens. Matter **10**, L55 (1988).

[8] S. L. Ren, J. J. Heremans, S. Vijeyaragunathan, T. D. Mishima, and M. B. Santos, J. Phys.: Condens. Matter **27**, 185801 (2015).

[9] Y. Xie, C. Le Priol, and J. J. Heremans, J. Phys.: Condens. Matter **28**, 495003 (2016).

[10] D. K. Ferry, A. M. Burke, R. Akis, R. Brunner, T. E. Day, R. Meisels, F. Kuchar, J. P. Bird, and B. R. Bennett, Semicond. Sci. Technol. **26**, 043001 (2011).

[11] M. Elhassan, J. P. Bird, R. Akis, D. K. Ferry, T. Ida, and K. Ishibashi, J. Phys.: Condens. Matter **17**, L351 (2005).

[12] B. Hackens, S. Faniel, C. Gustin, X. Wallart, S. Bollaert, A. Cappy, and V. Bayot, Phys. Rev. Lett. **94**, 146802 (2005).

[13] J. P. Bird, A. P. Micolich, D. K. Ferry, R. Akis, Y. Ochiai, Y. Aoyagi, and T. Sugano, Solid-State Electron. **42**, 1281 (1998).

[14] M. Katz, M. Ansmann, R. C. Bialczak, E. Lucero, R. McDermott, M. Neeley, M. Steffen, E. M. Weig, A. N. Cleland, J. M. Martinis, and A. N. Korotkov, Science **312**, 1498 (2006).

[15] M. Schlosshauer, Rev. Mod. Phys. **76**, 1267 (2004).

[16] D. Liang and X. P. A. Gao, Nano Lett. **12**, 3263 (2012).

[17] P. Lehnen, T. Schäpers, N. Kaluza, N. Thillosen, and H. Hardtdegen, Phys. Rev. B **76**, 205307 (2007).

[18] V. Chandrasekhar, D. E. Prober, and P. Santhanam, Phys. Rev. Lett. **61**, 2253 (1988).

[19] R. L. Kallaher, J. J. Heremans, N. Goel, S. J. Chung, and M. B. Santos, Phys. Rev. B **81**, 035335 (2010).

[20] M. Rudolph and J. J. Heremans, Phys. Rev. B **83**, 205410 (2011).

[21] R. L. Kallaher, J. J. Heremans, W. Van Roy, and G. Borghs, Phys. Rev. B **88**, 205407 (2013).

[22] P. Roulleau, T. Choi, S. Riedi, T. Heinzel, I. Shorubalko, T. Ihn, and K. Ensslin, Phys. Rev. B **81**, 155449 (2010).

[23] D. Liang, J. Du, and X. P. A. Gao, Phys. Rev. B **81**, 153304 (2010).

[24] T. Schäpers, V. A. Guzenko, M. G. Pala, U. Zülicke, M. Governale, J. Knobbe, and H. Hardtdegen, Phys. Rev. B **74**, 081301(R) (2006).

[25] K. T. Lin, Y. Lin, C. C. Chi, and J. C. Chen, Phys. Rev. B **84**, 235404 (2011).

[26] C. Texier and G. Montambaux, Phys. Rev. B **72**, 115327 (2005).

[27] T. Ludwig and A. D. Mirlin, Phys. Rev. B **69**, 193306 (2004).

[28] C. Texier, P. Delplace, and G. Montambaux, Phys. Rev. B **80**, 205413 (2009).

[29] M. Ferrier, A. C. H. Rowe, S. Guéron, H. Bouchiat, C. Texier, and G. Montambaux, Phys. Rev. Lett. **100**, 146802 (2008).

[30] C. Texier, Phys. Rev. B **76**, 153312 (2007).

[31] A. G. Huibers, M. Switkes, C. M. Marcus, K. Campman, and A. C. Gossard, Phys. Rev. Lett. **81**, 200 (1998).

[32] S. Faniel, B. Hackens, A. Vlad, L. Moldovan, C. Gustin, B. Habib, S. Melinte, M. Shayegan, and V. Bayot, Phys. Rev. B **75**, 193310 (2007).

[33] B. Hackens, S. Faniel, C. Gustin, X. Wallart, S. Bollaert, A. Cappy, and V. Bayot, Physica E **34**, 511 (2006).

[34] S. V. Iordanskii, Yu. B. Lyanda-Geller, and G. E. Pikus, Pis'ma Zh. Eksp. Teor. Fiz. **60**, 199 (1994) [JETP Lett. **60**, 206 (1994)].

[35] G. Bergmann, Int. J. Mod. Phys. B **24**, 2015 (2010).

[36] S. McPhail, C. E. Yasin, A. R. Hamilton, M. Y. Simmons, E. H. Linfield, M. Pepper, and D. A. Ritchie, Phys. Rev. B **70**, 245311 (2004).

[37] V. Deo, Y. Zhang, V. Soghomonian, and J. J. Heremans, Sci. Rep. **5**, 9487 (2015).

[38] G. Bergmann, Phys. Rep. **107**, 1 (1984).

[39] B. Doucot and R. Rammal, J. Phys. **47**, 973 (1986).

[40] E. Akkermans and G. Montambaux, *Mesoscopic Physics of Electrons and Photons* (Cambridge University Press, Cambridge, 2007).

[41] M. Treiber, C. Texier, O. M. Yevtushenko, J. von Delft, and I. V. Lerner, Phys. Rev. B **84**, 054204 (2011).

[42] K. K. Choi, D. C. Tsui, and K. Alavi, Phys. Rev. B **36**, 7751 (1987).

[43] W. Zawadzki and W. Szymanska, Phys. Status Solidi B **45**, 415 (1971).

[44] W. Zawadzki, J. Phys.: Condens. Matter **29**, 373004 (2017).

[45] T. Matsuoka, E. Kobayashi, K. Taniguchi, C. Hamaguchi, and S. Sasa, Jpn. J. Appl. Phys. **29**, 2017 (1990).

[46] E. Diez, Y. P. Chen, S. Avesque, M. Hilke, E. Peled, D. Shahar, J. M. Cerveró, D. L. Sivco, and A. Y. Cho, Appl. Phys. Lett. **88**, 052107 (2006).

[47] J. C. Licini, G. J. Dolan, and D. J. Bishop, Phys. Rev. Lett. **54**, 1585 (1985).

[48] J. J. Heremans, R. L. Kallaher, M. Rudolph, M. Santos, W. VanRoy, and G. Borghs, Proc. SPIE **9167**, 91670D (2014).

[49] S. Kettemann, Phys. Rev. Lett. **98**, 176808 (2007).

[50] S. Hikami, A. I. Larkin, and Y. Nagaoka, Prog. Theor. Phys. **63**, 707 (1980).

[51] G. J. Dolan, J. C. Licini, and D. J. Bishop, Phys. Rev. Lett. **56**, 1493 (1986).

[52] A. Zduniak, M. I. Dyakonov, and W. Knap, Phys. Rev. B **56**, 1996 (1997).

[53] C. W. J. Beenakker and H. van Houten, Phys. Rev. B **38**, 3232 (1988).

[54] Y. Kunihashi, M. Kohda, and J. Nitta, Phys. Rev. Lett. **102**, 226601 (2009).

[55] J. P. Bird, K. Ishibashi, D. K. Ferry, Y. Ochiai, Y. Aoyagi, and T. Sugano, Phys. Rev. B **51**, 18037 (1995).

[56] R. A. Jalabert, H. U. Baranger, and A. D. Stone, Phys. Rev. Lett. **65**, 2442 (1990).

[57] D. P. Pivin, A. Andresen, J. P. Bird, and D. K. Ferry, Phys. Rev. Lett. **82**, 4687 (1999).

[58] P. Mohanty and R. A. Webb, Phys. Rev. B **55**, R13452 (1997).

[59] P. Mohanty, E. M. Q. Jariwala, and R. A. Webb, Phys. Rev. Lett. **78**, 3366 (1997).

[60] T. Hiramoto, K. Hirakawa, Y. Iye, and T. Ikoma, Appl. Phys. Lett. **54**, 2103 (1989).

[61] D. Natelson, R. L. Willett, K. W. West, and L. N. Pfeiffer, Phys. Rev. Lett. **86**, 1821 (2001).

[62] B. L. Altshuler, M. E. Gershenson, and I. L. Aleiner, Physica E **3**, 58 (1998).

[63] S. J. MacLeod, K. Chan, T. P. Martin, A. R. Hamilton, A. See, A. P. Micolich, M. Aagesen, and P. E. Lindelof, Phys. Rev. B **80**, 035310 (2009).

[64] P. T. Coleridge, Phys. Rev. B **44**, 3793 (1991).

[65] K. H. Gao, G. Yu, Y. M. Zhou, W. Z. Zhou, T. Lin, J. H. Chu, N. Dai, D. G. Austing, Y. Gu, and Y. G. Zhang, Phys. Rev. B **79**, 085310 (2009).